6-2001

Multilamellar bodies as potential scattering particles in human age-related nuclear cataracts

K. O. Gilliland

C. D. Freel

C. W. Lane

W. C. Fowler

M. J. Costello

Molecular Vision 2000; 7:120-30 <http://www.molvis.org/molvis/v7/a18>
Received 19 February 2001 | Accepted 15 June 2001 | Published 22 June 2001

Multilamellar bodies as potential scattering particles in human age-related nuclear cataracts

Kurt O. Gilliland,[1] Christopher D. Freel,[1] C. Wesley Lane,[1] W. Craig Fowler,[2] M. Joseph Costello[1]

[1]Department of Cell and Developmental Biology, University of North Carolina at Chapel Hill, Chapel Hill, NC; [2]Department of Ophthalmology, Duke University Eye Center, Durham, NC

Purpose: To characterize within human age-related nuclear cataracts rare spherical objects covered by multiple membranes, termed multilamellar bodies (MLBs).

Methods: Adult human normal, transparent lenses were obtained from eye bank donors and age-related nuclear cataracts were obtained immediately after extracapsular extraction. Each sample was Vibratome sectioned fresh into 200 μm thick sections that were fixed and embedded for light or electron microscopy. Confocal images were recorded from sections stained with the lipid soluble dye, DiI.

Results: Light micrograph montages of the equatorial plane containing the fetal and embryonic nuclei were examined. Rare, but distinct, circular 1-3 μm diameter objects were observed consistently in the cataracts. These objects did not appear to be components of the complex intercellular interfaces. Serial sections indicated that the objects were spherical, or contained a spherical component. For about 20,000 fiber cell cross-sections in each lens, the frequency of MLBs was 10 times higher in cataracts than in the normal lens nuclei. Although extensive searching with the electron microscope was necessary, the size, circular profile and multiple layers of thin (5 nm) membranes easily identified the MLBs. Interiors of the MLBs displayed variable textures. Confocal images indicated that the coverings were enriched in lipid compared to the adjacent plasma membranes. The calculated density of the MLBs in the cataractous nuclei was about 3800/mm^3, which represents a volume fraction of 0.00003.

Conclusions: Because the MLBs are large compared to the wavelength of light, display interiors with variable staining textures and have lipid-rich coverings, they appear to be ideal candidates for large scattering particles that may contribute to the forward light scattering in nuclear cataracts.

The sources of light scattering in human nuclear cataracts are unknown. Many studies have suggested that the primary insult in age-related cataract formation is oxidative damage to cytoplasmic proteins and membranes [1,2]. Although oxidation may be the fundamental biochemical change leading to age-related degeneration of the lens, as well as other tissues, the initial biochemical steps occur on too small a scale to have a significant effect on the scattering of white light. In order to produce scattering particles of sufficient size, the oxidative changes must accumulate or initiate a cascade of physical changes that produce local fluctuations in refractive index. Numerous proposals for cellular changes have been described, such as the condensation of cytoplasmic proteins into heavy molecular weight aggregates [3].

Such hypotheses are useful conceptually for the interpretation of biomicroscopic, biochemical and ultrastructural data. However, identification of specific scattering particles in human cataracts corresponding to the predicted cellular alterations has proven elusive. Although high molecular weight aggregates of cytoplasmic crystallins have been documented extensively [4-6], the visualization of the aggregates has been difficult. The nuclear cytoplasm of well-preserved aged human lenses and most human nuclear cataracts is smooth and homogeneous by light and electron microscopy [7,8]. The few exceptions reported show a slight texturing of the cytoplasm that may represent crystallin aggregation and/or precipitation [9]. However, such texturing was present in only a fraction of the nuclear cataracts examined, suggesting that other sources of scattering are more important for the majority of nuclear cataracts [10].

For scattering particles to be generated, biochemical or cellular changes must produce refractive index fluctuations on a scale sufficient to interact with light. There are two main theoretical approaches that deal with the scale of the fluctuations. Based on modifications of the Rayleigh scattering theory of dilute solutions, Benedek [11] suggests that objects or density fluctuations larger than half the wavelength of light, or about 200 nm, will produce significant light scattering. The second theoretical approach, based on scattering from inhomogeneous materials, suggests that fluctuations on a smaller scale, down to 20 nm, may be significant [12,13]. Thus, a distinction can be made between small scattering particles, roughly 20-200 nm, and large scattering particles, 200-1000 nm and larger. Such a distinction is useful because it can help relate the geometry of the scattering particles to the observed scattering. For example, it has been suggested that age-dependent condensation of cytoplasmic proteins to form heavy molecular weight aggregates produces small irregular scattering particles that yield diffuse scattering at high angles, as

Correspondence to: M. Joseph Costello, PhD, Department of Cell and Developmental Biology, University of North Carolina at Chapel Hill, Chapel Hill, NC, 27599-7090; Phone: (919) 966-6981; FAX: (919) 966-1856; email: mjc@med.unc.edu

seen typically in slit-lamp images of normal aging lenses and nuclear cataracts [14,15].

The bimodal scattering model is consistent with the extensive analysis of the scattering of human donor lenses [15,16]. Both normal and cataractous human lenses were exposed to slits of white light and the scattering was recorded at various angles. The scattering profiles were modeled such that the backscattered light, contributing mainly to slit-lamp images, was produced by small scattering particles and the forward scattering was accounted for by large scattering particles. Significantly, the analysis suggested that the large scattering particles have an average diameter of about 1.4 µm and occupy a volume fraction less than 0.00005 [15,16].

In the present morphological analysis of human lens nuclei, we report objects that occur with a frequency consistent with that predicted by theoretical modeling [15,16]. These rare objects usually have a spherical core covered by multiple membrane layers and are thus termed multilamellar bodies (MLBs). With diameters often in the range of 1-3 µm, thick coverings of multiple membranes and variable staining densities in electron micrographs, our evidence suggests that MLBs are distinct from other vesicle-like profiles [7,17] and are sites of local refractive index variations. Because the MLBs are globular and have dimensions comparable to the wavelength of white light, they meet the criteria for large scattering particles that potentially produce significant forward scattering.

METHODS

Lenses: Five cataractous human nuclei (ages 72, 75, 81, 85, and 85) were obtained after extracapsular cataract extraction from the Duke University Eye Center (Durham, NC). These cataracts were transported to the University of North Carolina at Chapel Hill the day of surgery and were prepared for analysis. Five normal human eyes (ages 50, 59, 65, 66, and 71) were obtained from the North Carolina Eye and Human Tissue Bank (Durham, NC). These eyes were transported within

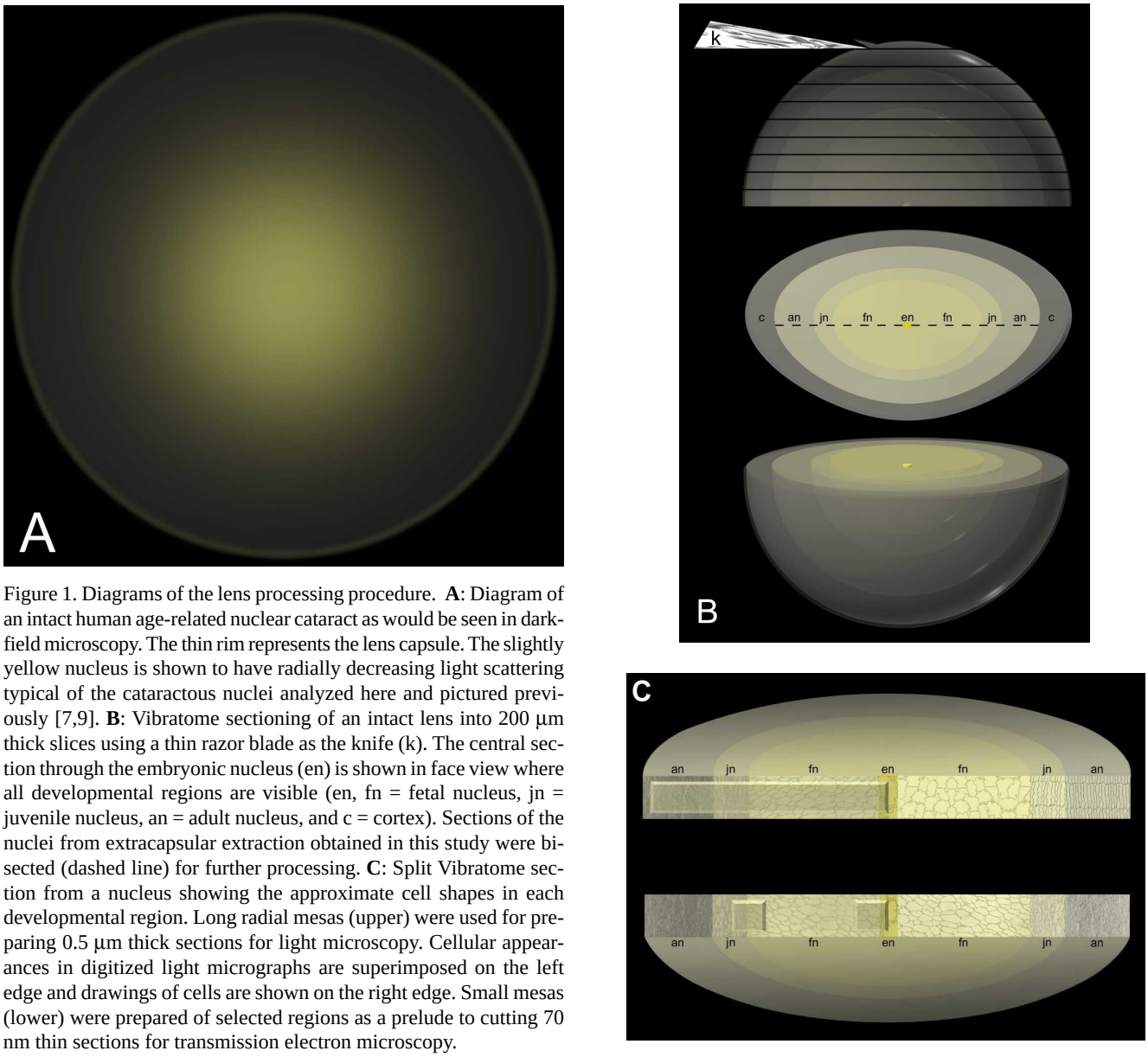

Figure 1. Diagrams of the lens processing procedure. **A**: Diagram of an intact human age-related nuclear cataract as would be seen in dark-field microscopy. The thin rim represents the lens capsule. The slightly yellow nucleus is shown to have radially decreasing light scattering typical of the cataractous nuclei analyzed here and pictured previously [7,9]. **B**: Vibratome sectioning of an intact lens into 200 µm thick slices using a thin razor blade as the knife (k). The central section through the embryonic nucleus (en) is shown in face view where all developmental regions are visible (en, fn = fetal nucleus, jn = juvenile nucleus, an = adult nucleus, and c = cortex). Sections of the nuclei from extracapsular extraction obtained in this study were bisected (dashed line) for further processing. **C**: Split Vibratome section from a nucleus showing the approximate cell shapes in each developmental region. Long radial mesas (upper) were used for preparing 0.5 µm thick sections for light microscopy. Cellular appearances in digitized light micrographs are superimposed on the left edge and drawings of cells are shown on the right edge. Small mesas (lower) were prepared of selected regions as a prelude to cutting 70 nm thin sections for transmission electron microscopy.

12 h of death to the University of North Carolina at Chapel Hill, where the transparent lenses were dissected from the globes and prepared for analysis in the same fashion as the cataracts. All specimens were collected following the tenets of the Declaration of Helsinki.

Donor lenses were pale yellow to yellow in color (using the scale for in vitro lenses by Chylack, et al. [18]) and were fully transparent to white light. When placed on a rectangular grid, the transparent lenses did not distort the image of the grid and they showed no cortical spokes or shades when viewed with oblique or darkfield illumination. The age-related cataractous nuclei showed yellow to dark yellow coloration [18] but were not brunescent. The nuclear scattering corresponded to a grade 2-3 on a scale 0-4 [18] and is therefore similar to the nuclear cataracts analyzed previously [7,9].

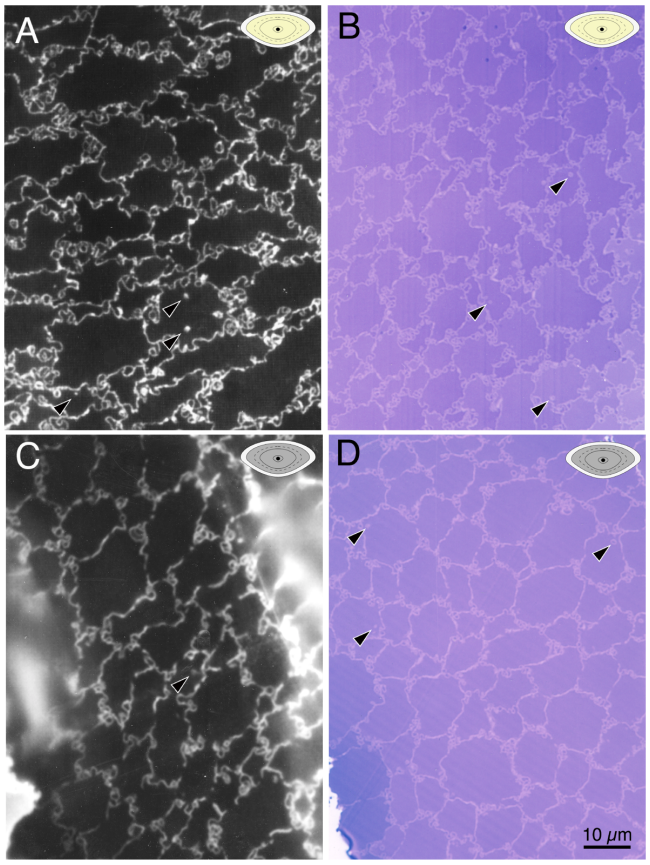

Figure 2. Microscopic images of embryonic fiber cells. A 50 year old normal transparent lens (**A**, **B**) and an 81 year old age-related nuclear cataract (**C**, **D**) are compared using two microscopic techniques. Lipid-containing membranes and circular profiles are visualized in a fluorescence microscope using the lipophilic stain, DiI (**A**, **C**), whereas similar fields of the same lenses are seen in histological sections stained with TBO (**B**, **D**). Many circular profiles are visible at the intercellular interfaces especially where three cells join. Only a few lipid-containing profiles are visible in the cytoplasm (arrowheads). The quantitative analysis shows that the normal lens has more profiles than the cataract, and most of the profiles are near intercellular interfaces. In the upper right corner of each image is a lens locator diagram (yellow for a normal lens and gray for a cataract) which contains a black dot to indicate which developmental region of the lens (see Figure 1B) is shown in the micrograph.

The equatorial diameter and anterior-to-posterior thickness of each lens was measured before being mounted with cyanoacrylate glue onto a metal sectioning tray. Lenses were covered with warm 2.5% agar, then submerged in Tyrode's salt solution (Sigma, St. Louis, MO) at 10 °C, and sectioned using a vibrating knife microtome (TPI Vibratome model 1000, St. Louis, MO) at an amplitude of 7, a speed of approximately 0.2 mm/s, and a cutting angle of 12° (Figure 1).

Light microscopy: Vibratome sections approximately 200 μm thick were fixed in 0.5% glutaraldehyde, 2% paraformaldehyde, and 1% tannic acid in 0.1 M cacodylate buffer (pH 7.2) for 12 to 18 h. Sections were washed with deionized distilled water for three 15-min washings, stained in 2% aqueous uranyl acetate in the dark for sixty min, washed with deionized distilled water for one 10-min washing, and then dehydrated through a graded ethanol series. Sections were infiltrated and embedded in LR White resin (Electron Microscopy Sciences, Ft. Washington, PA). Histological sections (0.5 μm thick) were cut along one half of the equatorial axis (Figure 1C) and mounted on glass slides. Mounted sections were stained with toluidine blue oxide (TBO), cover slipped, and examined with an Olympus BX40 (OPELCO, Dulles, VA) brightfield microscope.

Transmission electron microscopy: Vibratome sections approximately 200 μm thick were fixed in 2.5% glutaraldehyde, 2% paraformaldehyde, and 1% tannic acid in 0.1 M cacodylate buffer (pH 7.2) for 12 to 18 h. Sections were washed with 0.1 M cacodylate for three 15-min washings, treated with cold 0.5% osmium tetroxide for sixty min, washed with deionized distilled water for three 15-min washings, washed once with 50% ethanol for 5 min, stained in 2% uranyl acetate (ethanol-based) in the dark for thirty min, and then dehydrated through a graded ethanol series. Sections were infiltrated and embedded in an epoxy resin. Thin sections (70 nm) were cut from mesas raised along various locations of the equatorial

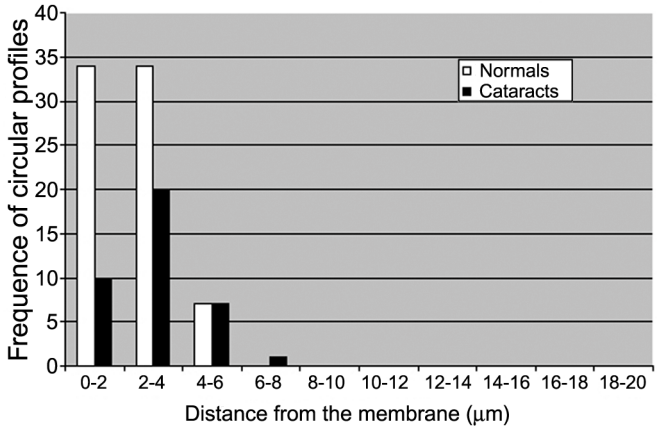

Figure 3. Distance mapping of profiles from the membrane. Quantitative measurements were made from four normal lenses and four cataracts. Circular profiles were counted in random areas (7000 μm^2) of embryonic and fetal nuclear regions, and the distance between each profile and the cell membrane was measured. Results demonstrate that the normal lens contains more circular profiles than the cataract, although the difference is not statistically significant. These profiles are predominantly located within 4 μm of the cell membrane.

axis (Figure 1C) and stained with uranyl acetate and lead citrate for viewing at 80 kV on a JEOL 200CX (JEOL, Inc., Peabody, MA) or a Philips-FEI Tecnai 12 (FEI Company, Hillsboro, OR) transmission electron microscope.

Confocal and fluorescence light microscopy: Sections of 2 to 4 µm were cut from LR White embedded Vibratome sections on a microtome and stained with the lipophilic dye, DiI (1,1-dioctadecyl-3,3,3',3'-tetramethylindocarbocyanine perchlorate; Molecular Probes, Inc., Eugene, OR) following the procedures published previously [17]. Optical sectioning on a Zeiss LSM-410 (Carl Zeiss, Inc., Thornwood, NY) laser scanning confocal microscope was used to examine the tissues. The conventional fluorescence images were taken with a Zeiss Axioplan 2 microscope.

Quantitative analysis: Light micrograph negatives were scanned using a Polaroid Sprintscan 35 and color corrected using Adobe Photoshop version 5.02 (San Jose, CA). Cells and circular profiles were counted, and the distance between these circular profiles and the nearest cell membrane was

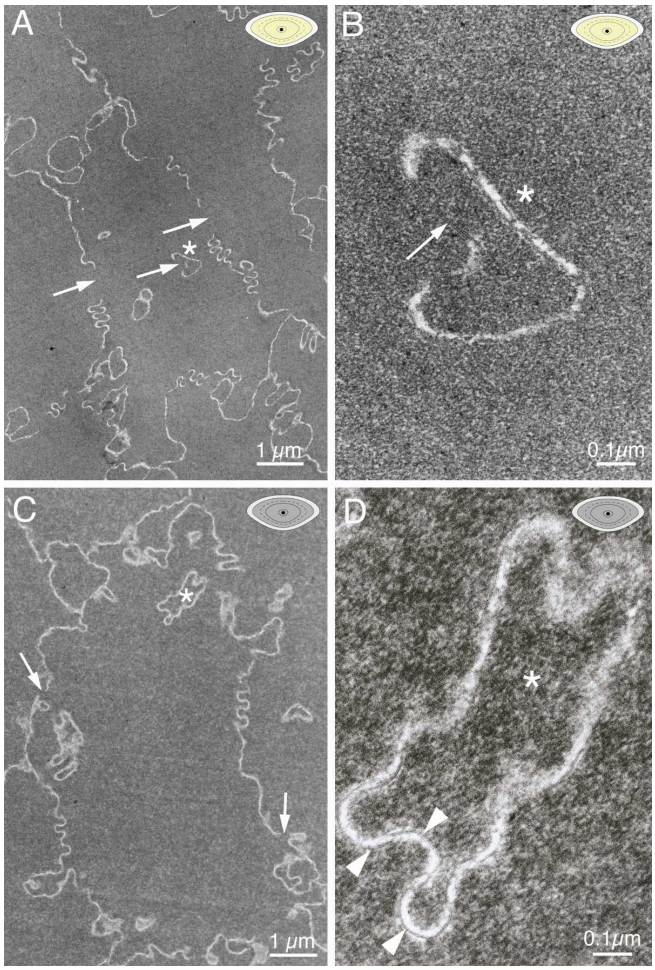

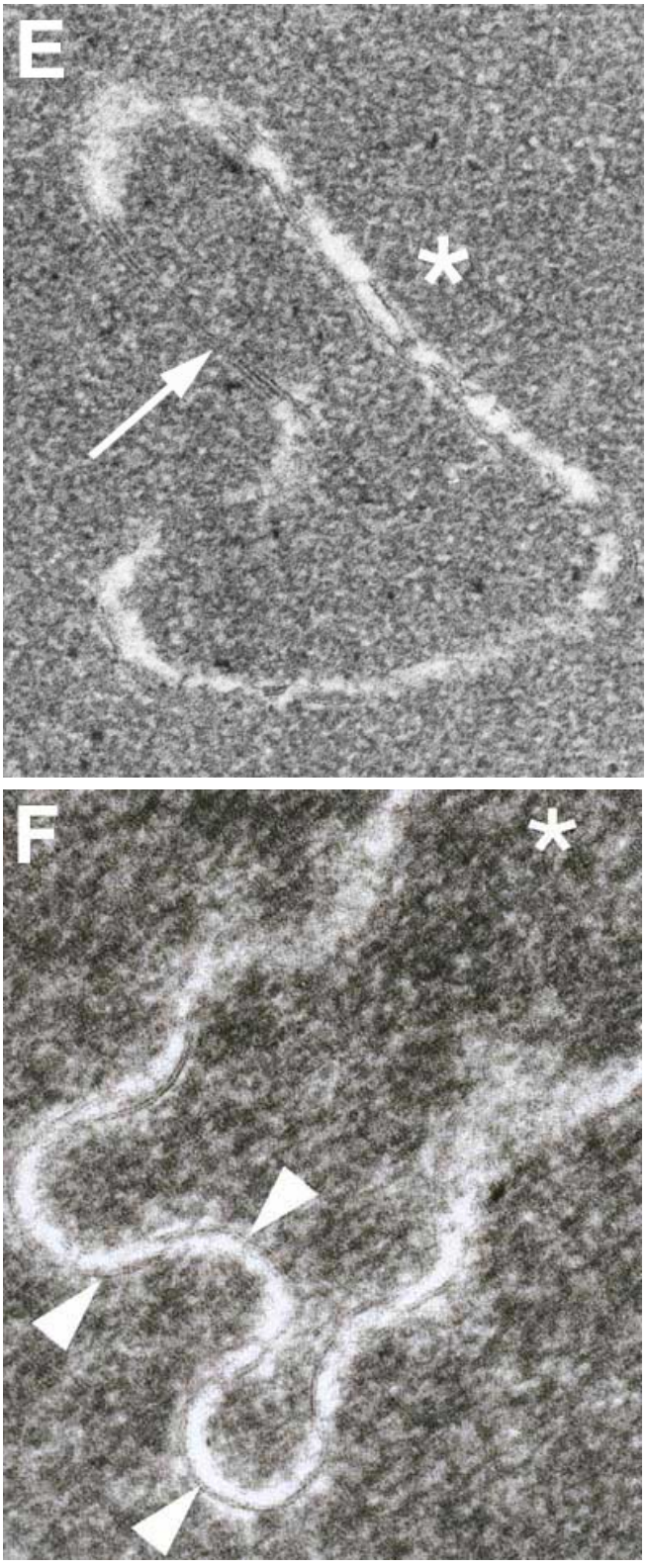

Figure 4. Electron micrographs of normal and cataractous lenses. A 50 year old normal transparent lens (**A**, **B**) and an 81 year old age-related nuclear cataract (**C**, **D**) are compared using transmission electron microscopy. Electron micrographs at low magnification (**A**, **C**) are consistent with light micrographs in Figure 2. High magnification images (**B**, **D**) of circular profiles (*) in the cytoplasm confirm that they are bounded by paired membranes including a gap junction (arrows), implying that they are derived from projections of the cellular interface rather than isolated vesicles. Square array junctions containing MIP/Aquaporin0 channels are marked by arrowheads (**D**). **E** and **F** are further magnifications of the area of interest near the "*" from **B** and **D**. In the upper right corner of images **A**-**D** is a lens locator diagram (light gray for a normal lens and dark gray for a cataract) which contains a black dot to indicate which developmental region of the lens (see Figure 1B) is shown in the micrograph.

measured with NIH Image version 1.62 (National Institutes of Health, Bethesda, MD), enhanced with a subroutine provided by Dr. John Russ (North Carolina State University, Raleigh, NC). MLBs were counted in histological sections of greater than 1 mm^2 for each lens. The data were analyzed statistically using StatView version 5.0 (SAS Institute, Inc., Cary, NC), employing the non-parametric Mann-Whitney test, appropriate for data with small n, which shows trends that were considered significant for $p<0.05$. The number of MLBs per area was extrapolated to a number per volume using the Floderus equation [19].

RESULTS

Cytoplasmic profiles in normal and cataractous lenses: Vesicle-like profiles surrounded by cytoplasm have been suggested as a source of scattering in nuclear cataracts [17]. Such profiles within the cytoplasm were examined quantitatively in order to evaluate their potential role as scattering particles and to distinguish them from MLBs. Examples of the profiles are visible by fluorescence and brightfield light microscopy (Figure 2). Consistent with transmission electron microscopic comparisons published previously [7,9], the embryonic and fetal nuclear regions of normal and cataractous lenses are morphologically indistinguishable. Note specifically that the cytoplasm of the cells in each region is smooth and homogeneous, particularly evident for the embryonic nucleus in the TBO-stained cytoplasm in Figure 2B and Figure 2D. Likewise, the membranes and cellular interfaces of the normal lens (specifically labeled in Figure 2A and seen in negative contrast in Figure 2B) appear similar to those of the cataract. Both have similar complexity and similar numbers of finger-like projections from one cell into an adjacent cell. In these images the vesicle-like profiles often appear to be sections of the globular distal ends of cell-to-cell projections where the connection to the nearby cell membrane is not evident (Figure 2).

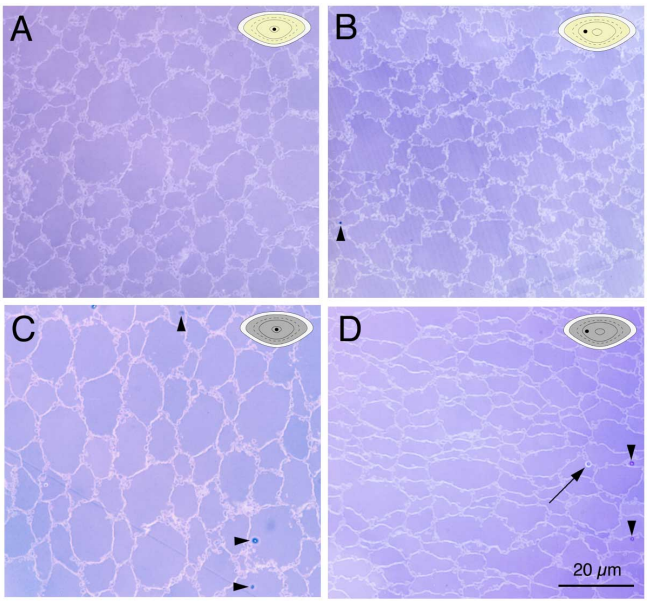

Figure 5. Light micrographs of normal and cataractous lenses. The embryonic (**A**) and fetal (**B**) nuclear regions of a normal lens appear virtually indistinguishable from the embryonic (**C**) and fetal (**D**) nuclear regions of a cataract. A multilamellar body (MLB), however, can be seen in **D** (arrow). MLBs occur both in normal lenses and in cataracts, but they occur with 10 times greater frequency in cataracts. Sectioning and staining artifacts are noted by arrowheads. The stain color and refractile properties visible during focusing readily distinguish the stain artifacts from MLBs. In the upper right corner of each image is a lens locator diagram (yellow for a normal lens and gray for a cataract) which contains a black dot to indicate which developmental region of the lens (see Figure 1B) is shown in the micrograph.

The vesicle-like profiles within the cell cytoplasm are most often located near cellular interfaces, with only a very few being located in the center of the cell away from the plasma membrane. The distribution of profiles was measured by examining approximately 7,000 μm^2 of randomly selected tissue in the embryonic and fetal nuclear regions in each of four normal lenses and four cataractous nuclei. The quantitative data demonstrate that these cytoplasmic profiles are predominantly within 4 μm of the nearest cell membrane (Figure 3). In summary, 177 cells from normal lenses were found to contain the observed 75 circular profiles (an average of 0.43 profiles per cell) and 174 cells from cataractous nuclei were found to contain the observed 38 profiles (an average of 0.23 profiles per cell, Table 1).

High magnification electron micrographs reveal that the circular profiles are bounded by paired, not single, membranes (Figure 4). Therefore, these profiles are most likely cross and oblique sections of finger-like projections derived from the

Table 1. A comparison of cytoplasmic profile frequency in normal and cataractous nuclei

Normal Nuclei

Age (years)	Profiles	Cells	Profiles/Cell
50	21	62	0.34
59	9	27	0.33
66	15	48	0.31
71	30	40	0.75
Total	75	177	
Mean ± SD			0.43 ±0.21

Cataractous Nuclei

Age (years)	Profiles	Cells	Profiles/Cell
75	7	53	0.13
81	12	39	0.31
85(a)	10	33	0.30
85(b)	9	49	0.18
Total	38	174	
Mean ± SD			0.23 ±0.09

Normal and cataractous nuclei contain varying numbers of circular profiles. In this sample of about 7,000 μm^2 of the embryonic/fetal nuclear regions in each lens, the normal nuclei have more profiles per cell than the cataracts, but the difference is not statistically significant ($p=0.11$).

cellular interface rather than isolated cytoplasmic vesicles. The profiles vary in size but are commonly in the range of 0.2-0.5 µm in diameter. The interiors of the profiles are similar to the surrounding cytoplasm. Although a greater number of profiles was observed in normals, statistically there was no difference between the number of cytoplasmic profiles in the normal and the cataractous nuclei (p=0.11).

Multilamellar bodies: Extensive examination of montages of TBO-stained histological sections revealed the presence of rare circular structures that were distinct from the cytoplasmic profiles described above (Figure 5). Many of the objects were nearly perfect circles with wide clear borders (Figure 5D, arrow), were significantly larger than the cytoplasmic profiles, and were not necessarily close to the cell interfaces. Once these objects were recognized as unique structures, sections from ten lenses (five normal and five cataracts) were searched thoroughly at high magnification in the light microscope and using printed montages. Figure 5 illustrates the approximate frequency of the circular objects; that is, approximately one object was visible in a field of several hundred fiber cells cut in cross-section in the equatorial plane. Many of the objects appeared to be clusters or close associations of similar structures (Figure 6). While the mean diameter of these structures was 2.4 µm, a wide range of diameters was observed because the sections of individual MLBs were captured at different planes within their spherical shapes. In

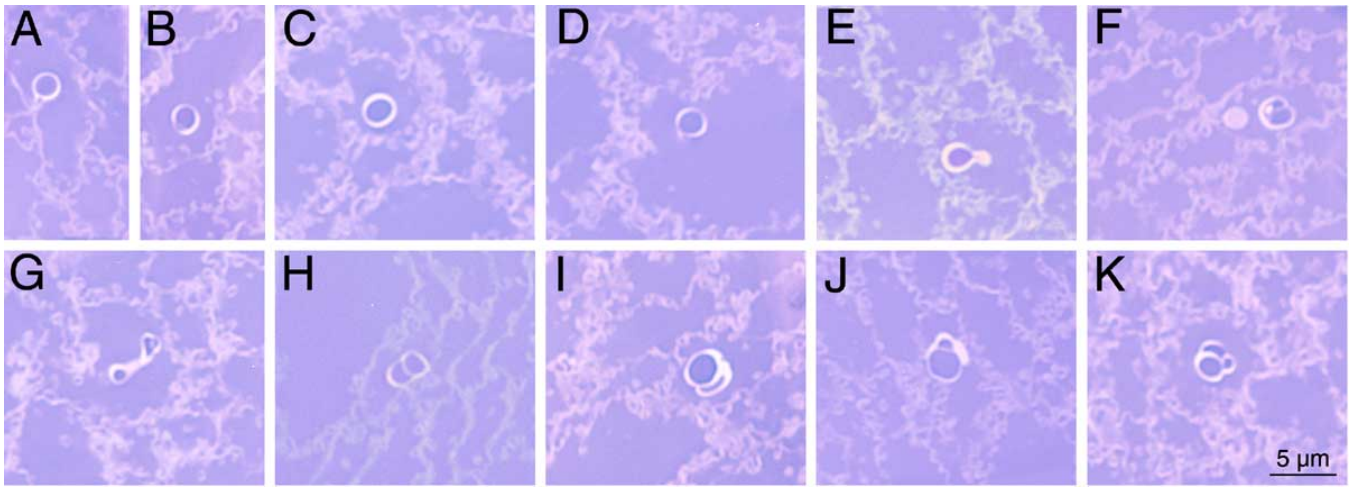

Figure 6. Gallery of light micrographs. These MLBs from the fetal nucleus display varying geometrical patterns. MLBs in **A**, **B**, **C**, and **D** are circular. The MLB in **E** shows a small protrusion. MLBs in **F** through **K** display doublet and even triplet structures.

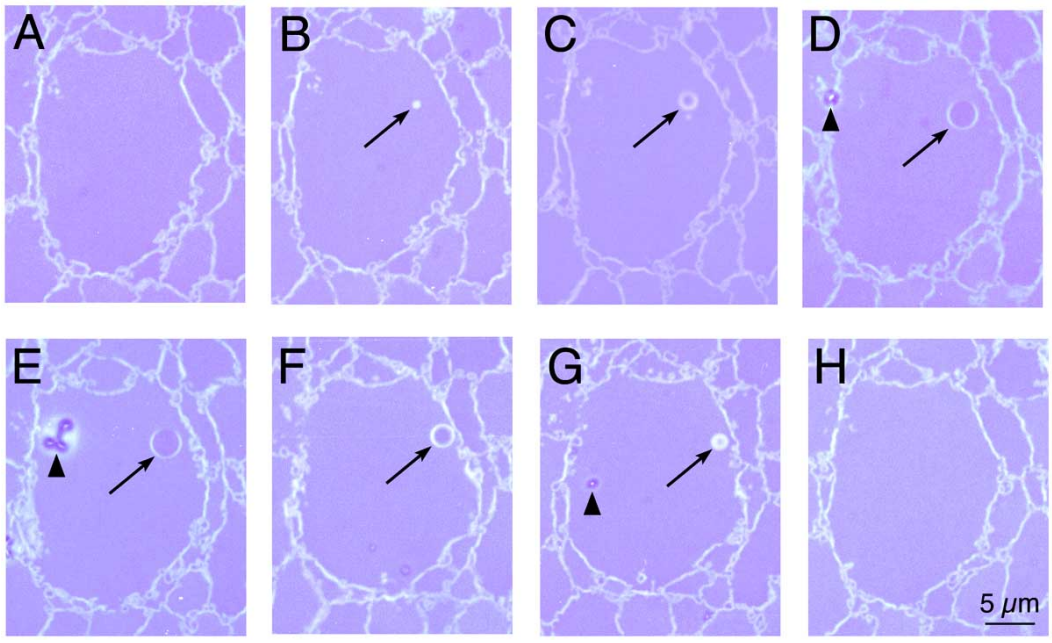

Figure 7. Serial sections of an MLB. Serial sections of an MLB in a cell in the embryonic nucleus. The MLB is not present in **A** or **H**. Based on 0.5-µm-thick light microscopy serial sections, the MLB (arrow) increases in size in **B** through **D**, achieving its widest diameter (3.4 µm) in **E** and decreases in size in **F** and **G**. The appearance of this typical MLB in serial sections suggests that its overall shape is spherical. The arrowheads indicate sectioning/staining artifacts.

addition, these structures appeared within the cytoplasm, as well as near the cellular interfaces, at ten times greater frequency in cataracts compared to normal lenses.

To establish the hypothesized spherical geometry of a majority of the unique structures, one structure was traced through eight 0.5 µm sections arranged in a serial pattern (Figure 7).

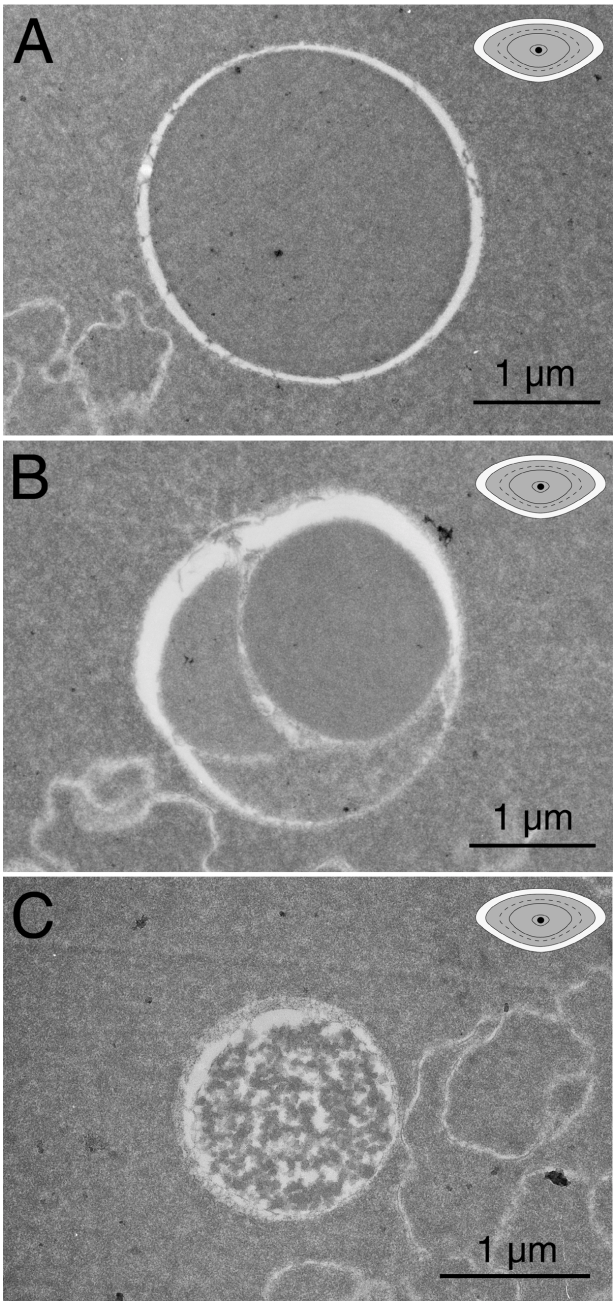

Figure 8. Gallery of transmission electron micrographs. TEMs are consistent with light micrographs. At about 20,000 times magnification, MLBs display variable cytoplasmic textures and unusual geometric patterns. **A**: Circular profile of an MLB with an interior that is smoother than the surrounding cytoplasm. **B**: Complex MLB with three domains, each with a different stain density and texture. **C**: A circular profile containing an irregular network of highly condensed strands. In the upper right corner of each image is a gray lens locator diagram which contains a black dot to indicate which developmental region of the lens (see Figure 1B) is shown in the micrograph.

In the first section, the circular structure is not present (Figure 7A), while in the second, third, and fourth serial sections (Figure 7B-D), it appears to be growing larger, achieving its maximum diameter of 3.4 µm in the fifth section (Figure 7E). In the sixth and seventh sections (Figure 7F-G), it becomes smaller until finally in the eighth section (Figure 7H) it is no longer present.

Thin section transmission electron micrographs show that these unique bodies vary not only in shape but also in cytoplasmic texture (Figure 8). Whereas some of these structures exhibit a smooth interior similar to the surrounding cytoplasm (Figure 8A), others exhibit differing degrees of texturing and variable stain density in different areas (Figure 8B). Electron micrographs also reveal that in some of these spherical structures, the texture can be extensively condensed or reorganized so as to appear totally different from the surrounding cytoplasm (Figure 8C).

High magnification electron micrographs establish that these large spherical bodies have multilamellar membranes (Figure 9). Unlike finger-like projections or circular profiles, which consistently exhibit paired membranes, these large spherical objects are bounded by three to eight bilayer mem-

Table 2. Comparison of the frequency of MLBs

Normal lenses

Age (years)	MLBs	Area (mm^2)	MLBs/(mm^2)
50	0	1.74	0.0
59	6	1.03	5.8
65	1	1.52	0.7
66	1	1.60	0.6
71	0	2.00	0.0
Total	8	7.89	
Average			1.4

Cataractous lenses

Age (years)	MLBs	Area (mm^2)	MLBs/(mm^2)
72	31	1.48	20.9
75	6	1.33	4.5
81	16	1.63	9.8
85(a)	9	1.36	6.6
85(b)	21	2.02	10.4
Total	83	7.82	
Average			10.4

Greater than 1 mm^2 of fetal and embryonic nuclear regions were searched in each of 5 normal and 5 cataractous nuclei. A total of 83 MLBs in the cataracts, but only 8 in the normal lenses, were observed in about 8 mm^2 of histological sections examined from each type of specimen. Comparing the MLBs per unit area examined, the cataracts exhibited 10.4 MLBs/mm^2, whereas the normal lenses showed only 1.4 MLBs/mm^2. The Mann-Whitney statistical test for small n supports the trend that the cataracts have more MLBs than the normals (p=0.016).

branes. The geometry of the packing of the layers is distinctly different from the typical plasma membranes and intercellular junctions in the same region (Figure 10). The membrane thickness, 5 nm, of the multilayered membranes (Figure 10A,C,E) suggests that they contain relatively little protein compared to gap junctions (Figure 10B,D,F) or undulating membrane domains rich in MIP/Aquaporin0 (Figure 10G,H). The undulating membranes at typical cellular interfaces are formed by paired membranes (Figure 10H) and are thus distinct from the multilamellar coverings of the unique spherical multilamellar bodies. The high lipid content of the MLBs is supported by the confocal images employing a lipid-soluble dye, DiI (Figure 11). Lipid-containing membrane pairs at cellular interfaces and in circular profiles are easily visualized (Figure 11, arrowheads). The increased intensity and distinctive geometry of the MLBs (Figure 11B-D) strongly suggest that the layers are rich in lipids. Serial confocal optical sections through these intensely fluorescent bodies also indicate that many are nearly perfect spheres (data not shown).

Quantification of the distribution of MLBs was accomplished by examining more than 1 mm^2 of fetal and embryonic nuclear regions in 0.5 µm TBO-stained sections of each of 5 normal lenses and 5 cataractous lenses. This thorough examination revealed 83 MLBs in the cataracts but only 8 in the normal lenses. All five of the cataracts contained MLBs, whereas two of the five normal lenses contained no observable MLBs. The cataracts exhibited 10.4 of these spherical structures per square millimeter of tissue examined, whereas the normal lenses showed only 1.4. The Mann-Whitney statistical test for small n suggests that the difference is significant (p=0.016, Table 2). To predict the number of MLBs that would be present per unit volume, the Floderus equation was used [19]. The numerical density of MLBs was determined by relating the number of structures per unit area to the section thickness and structure diameter. In 1 mm^3, the cataract is calculated to contain 3887 MLBs, whereas the normal lens is likely to contain just 382. The total volume of the fetal and embryonic nuclei of a typical aged human lens is about 24 mm^3 [20], suggesting that the inner regions of the nuclear cataracts examined contain over 90,000 MLBs. Since the average volume of an MLB is 7.24 μm^3, it was determined, based on the numerical density, that the MLBs occupy a volume fraction of 0.00003 of the cataract, with the normal lenses having

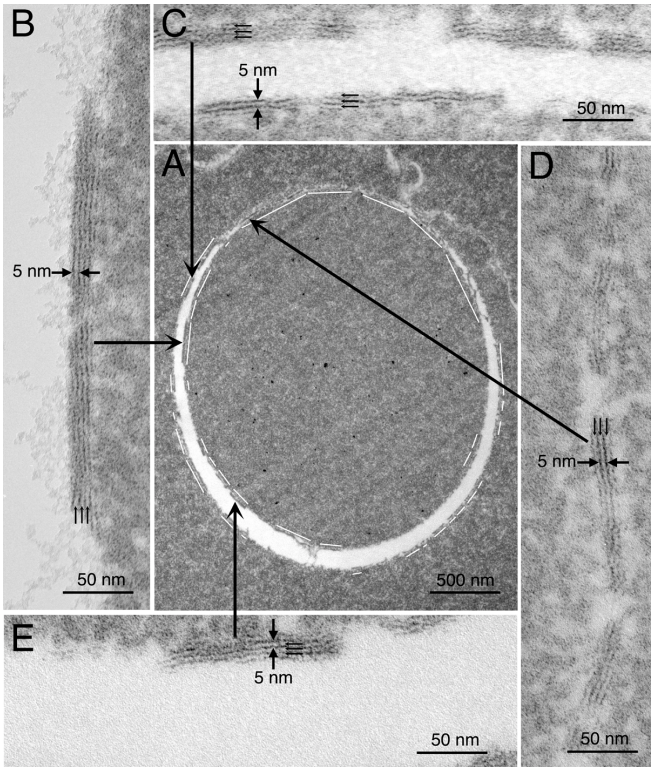

Figure 9. Electron micrographs of an MLB. Transmission electron micrographs of an MLB in a cell of the embryonic nucleus with high magnification views of membranes. Electron micrographs of one MLB (**A**) with insets (**B**, **C**, **D**, **E**) displaying multiple layers in different locations of the MLB. Although only a small portion of the complete layer is preserved, the geometry of the packing of the layers is distinctly different from typical membranes and junctions in the same region. The multilayered regions consistently produce a membrane thickness of 5 nm or less. The small membrane thickness is consistent with high lipid content. The white segmented line surrounding the MLB in **A**indicates the length and location of the visible multilayered lipid membranes within the space forming the circular border of the MLB. Short parallel arrows mark the hydrophobic interiors of adjacent lipid bilayers within multilamellar stacks.

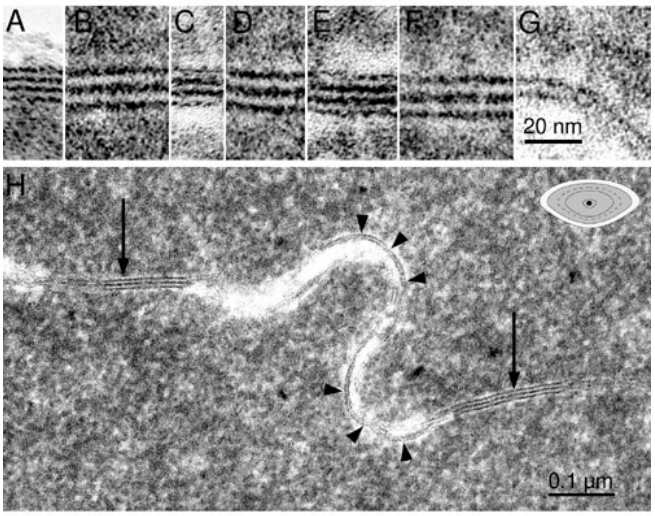

Figure 10. Comparisons of membranes by TEM. High-magnification transmission electron micrographs allow comparison of membrane thickness and staining patterns. The multilayered regions in **A**, **C**, and **E** are segments of multilayered membranes from MLBs, each containing three bilayers. The 5-nm distance from one lipid layer to another in these MLB membranes is probably too small to accommodate lens integral membrane proteins. The gap junctions in **B**, **D**, and **F** are 16 nm thick, and the single membrane in **G** (typical for square array junctions containing MIP/Aquaporin0) is 7 nm thick. These membranes are typical of the undulating membranes pictured in **H** (arrowheads). **A**, **C**, and **E** are taken from different segments of the MLB in Figure 9. Gap junctions in **B**, **D**, and **F** are taken from different gap junctions, two of which are shown in **H**(arrows).

a fraction 10 times smaller (Table 3).

DISCUSSION

The normal and cataractous lenses examined here with confocal and brightfield light microscopy are essentially indistinguishable in the embryonic and fetal nuclear regions. The cells of both the normal lenses and the cataracts contain smooth cytoplasm surrounded by membranes of similar complexity. Membranous profiles within the cytoplasm were also similar in number and appearance (Figure 2). In contrast, confocal images, employing the lipid fluorescent dye, DiI, were reported to show a markedly higher number of cytoplasmic profiles in nuclear cataractous lenses and almost no profiles in aged normal lenses [17]. A clear explanation of the differences in our study compared to the earlier report is not obvious. Three possible explanations based on sampling are (a) the normal lenses show such a low density of profiles (about 0.4 profile per cell; Table 1) that certain regions may show no profiles, (b) fiber cells cut obliquely may expose the large number of profiles at the complex intercellular interface, and (c) the sample population of cataracts is sufficiently small in both studies that distributions of profiles that are exceptional, rather than representative, may be given greater weight. A further difference in the studies should be noted. The profiles in the confocal study were interpreted as lipid vesicles [17]. Lipid vesicles are typically bounded by single membranes, whereas our transmission electron microscopic results clearly demonstrate that the cytoplasmic profiles we observed are bounded by paired membranes (Figure 4). The transmission electron microscope images also suggest that cytoplasmic profiles are derived from the plasma membranes because the paired membranes display characteristic undulations and gap junctions identical to those observed at cellular interfaces [21,22]. Based on the close proximity of the profiles to the cell surfaces (Figure 3) and on the demonstration in thick sections that finger-like projections of nuclear fiber cells are present in monkey lenses [23] and human lenses [24], the profiles are most likely intercellular projections rather than lipid vesicles. The distinguishing features of the cytoplasmic profiles include their paired membranes, similar numbers in normal lenses compared to cataracts, similar staining density of their interiors with the adjacent cytoplasm and consistent size, typically 0.2-0.5 µm diameter [7,20].

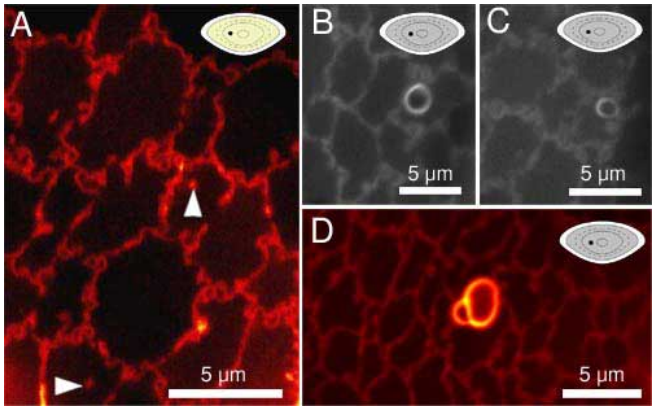

Figure 11. Comparison of normal and cataractous lenses. MLBs can be seen in cataractous tissue by laser scanning confocal microscopy using the lipid dye, DiI. Optical sectioning reveals lipid structures (**B**-**D**) of the same size and morphology as those examined by light and transmission electron microscopy, while the normal lenses typically contained no MLBs (**A**). Circular profiles (arrowheads in **A**) are distinguished from the obvious MLBs in **B**-**D**. In the upper right corner of each image is a lens locator diagram (yellow for a normal lens and gray for a cataract) which contains a black dot to indicate which developmental region of the lens (see Figure 1B) is shown in the micrograph.

TABLE 3. PREDICTION OF THE NUMBER OF MLBS PER UNIT VOLUME

	Normal	Cataract
N_V (MLBs/mm^3)	382	3887
V_{MLB}/mm^3	0.000003	0.00003

The Floderus equation was used to determine the numerical ensity (N_V) of the MLBs. The number of MLBs per unit area, the section thickness (0.5 µm), and the average diameter of an MLB (2.36 µm) led to a determination that there are 10 times as many MLBs in the cataract than in the normal lens. These calculations are based on:

$$N_V = N_A/(T + d - 2h)$$

where

N_V = Number of profiles of a feature/unit test volume (i.e., numerical density)
N_A = Number of profiles of a feature/unit test area (measured, MLBs/mm^2)
T = Section thickness = 0.5 \mu m (measured)
d = Profile diameter = 2.39 \mu m (measured average)
h = Height of the cap = 1/3 T (calculated)

Height of the cap (the smallest observed profile in the section) serves as a correction for the small polar regions of a sphere, which become lost to the eye since they are grazed during sectioning and therefore are only present in part of one section. For further information on the Floderus equation, see Bozzola and Russell [19].

Whereas circular profiles occur with high frequency in normal and cataractous lenses, there are larger spherical structures that seldom occur and are therefore difficult to observe in microscopic preparations. Extensive searching revealed, however, typically spherical structures wrapped in multiple layers of membranes, which we have termed multilamellar bodies, or MLBs, because the layers are not typical of other membranous structures and the objects appear to be isolated distinct globular bodies embedded within the nuclear fiber cells. In summary, the features that characterize the MLBs include multiple thin membranes, ten times greater frequency in the nuclear cataracts compared to the normal lenses, separation from the cell plasma membrane with interiors that have variable staining density, and an average diameter of 2.4 µm.

Based on their geometrical patterns, smooth contours, and multiple layers of lipid, MLBs appear to be distinct from the edge processes and interdigitations that characterize aged nuclear fiber cells [20,22]. The size of MLBs (commonly 1-3 µm diameter) and the variable appearance of their interiors compared to the adjacent fiber cell cytoplasm suggest that they might be a significant source of light scattering in nuclear cataracts. Van den Berg [15] suggested that particles larger than the wavelength of light could control forward light scattering. In particular, he hypothesized that particles of a mean radius

of 692 nm (mean diameter of 1.38 μm), should they exist, would be significant sources of forward light scattering [15]. Importantly, van den Berg [15,16] used a mathematical model to calculate that these large particles would need only to occupy a volume fraction between 0.000003 [15] and 0.000006 [16] of the donor lenses he examined in order to produce the significant forward scattering he observed. Our results indicate that, while MLBs occupy about 0.000003 of the volume of the normal human lens, they occupy as much as 0.00003 of the equivalent volume of the cataracts. This is similar to the volume fraction of 0.00005 occupied by the large particles in the only nuclear cataract reported by van den Berg [15,16]. This remarkable agreement between the size and volume fraction of the large scattering particles predicted by mathematical modeling [15,16] and our observations for MLBs further suggest that the MLBs should be considered as likely sources of nuclear light scattering.

The formation of MLBs must certainly be a complex process. Either by faulty fiber cell differentiation or simply by aging, fiber cells might become sufficiently dehydrated to compact excessively, causing a decrease in cell volume and therefore excess membrane surface area. This compaction would bring complex intercellular processes into close proximity [25]. Localized cell disruption, perhaps by oxidative damage to membranes [26], could lead to cell fragments within the fiber cell cytoplasm. During cellular "housekeeping", these excess pockets of membrane might pinch off and coil up to form spherical bodies wrapped in multiple layers of lipids. It should be noted that multiple layers of thin membranes have been reported for human lenses in regions of cell disruption [27] and in a rat model for high oxidative stress [28]. Furthermore, a number of reports describe punctate opacities containing lipids [29-31] and calcium [32]. None of the structures of these opacities were similar to the MLBs and none were shown to be in the fetal and embryonic nuclei. Other punctate opacities within the nucleus have recently been reported for genetic mutations of connexin [33,34] and called zonular nuclear pulverulent cataracts. The ultrastructures of these opacities have not been determined. It should be emphasized that the discrete, punctate opacities in the literature, some of which are in the 1-10 μm size range, are distinctly different from the MLBs described here which are not visible by eye or biomicroscopic examination and, importantly, human nuclear age-related cataracts do not normally display punctate opacifications.

MLBs are unique because they are large particles that are bound by multiple lipid layers and they often contain unusual internal textures. The coverings of MLBs, composed of 3 or 8 layers of tightly packed lipids, display an unusually thin interlayer spacing of about 5 nm. This thickness is probably too small to accommodate integral membrane proteins (Figure 10), such as those in the connexin or MIP/Aquaporin0 families. Therefore, it is unlikely that these MLBs are derived from gap junctions or square array junctions [35-37]. Instead, it is likely that the MLBs form by the redistribution of lipid components of the membrane into a thick shell that could isolate the MLB interior. Differential aging of the MLB interiors, due perhaps to the absence of channels and communicating junctions, may account for the variable staining densities observed in electron micrographs (Figure 8).

Although the number of MLBs observed is quite small, the frequency of MLBs in the cataracts, compared to the normal lenses, suggests that they should be considered as potential scattering particles. Because the sample populations are not age-matched, we cannot rule out the possibility that aging is a factor in the appearance of the MLBs. Regardless of their etiology, their distinctive internal structure, compared to the fiber cytoplasm, suggests that they are sources for local fluctuations in refractive index. The correspondence of the size and frequency of the MLBs to the large particles predicted theoretically gives additional support to the conclusion that the MLBs are potentially major sources of scattering in nuclear cataracts, even though at present we have no direct evidence that the MLBs scatter light. Further studies are needed to evaluate how significant the potential scattering particles are in the multifactorial process of nuclear cataract formation. The contribution that MLBs make to the scattering from human age-related cataracts will be better understood when their mechanism of formation is described, their chemical composition is defined, their distribution throughout the nucleus has been determined and their capacity to produce the observed scattering is confirmed in theoretical modeling studies of nuclear cataracts.

ACKNOWLEDGEMENTS

We thank Hal Mekeel for excellent electron microscopy assistance. Presented in part at the 1998 and 1999 Annual Meetings of the Association for Research in Vision and Ophthalmology, Ft. Lauderdale, Florida. This project was supported by NIH-NEI Research Grant EY08148 (UNC) and Core Grant EY05722 (Duke University).

REFERENCES

1. Spector A. The search for a solution to senile cataracts. Proctor lecture. Invest Ophthalmol Vis Sci 1984; 25:130-46.
2. Truscott RJ. Age-related nuclear cataract: a lens transport problem. Ophthalmic Res 2000; 32:185-94.
3. Benedek GB. Cataract as a protein condensation disease: the Proctor Lecture. Invest Ophthalmol Vis Sci 1997; 38:1911-21.
4. Jedziniak JA, Kinoshita JH, Yates EM, Hocker LO, Benedek GB. On the presence and mechanism of formation of heavy molecular weight aggregates in human normal cataractous lenses. Exp Eye Res 1973; 15:185-92.
5. Jedziniak JA, Kinoshita JH, Yates EM, Benedek GB. The concentration and localization of heavy molecular weight aggregates in aging normal and cataractous human lenses. Exp Eye Res 1975; 20:367-9.
6. Jedziniak JA, Nicoli DF, Baram H, Benedek GB. Quantitative verification of the existence of high molecular weight protein aggregates in the intact normal human lens by light-scattering spectroscopy. Invest Ophthalmol Vis Sci 1978; 17:51-7.
7. Al-Ghoul KJ, Lane CW, Taylor VL, Fowler WC, Costello MJ. Distribution and type of morphological damage in human nuclear age-related cataracts. Exp Eye Res 1996; 62:237-51.
8. Al-Ghoul KJ, Costello MJ. Light microscopic variation of fiber cell size, shape and ordering in the equatorial plane of bovine

and human lenses. Mol Vis 1997; 3:2 .
9. Al-Ghoul KJ, Costello MJ. Fiber cell morphology and cytoplasmic texture in cataractous and normal human lens nuclei. Curr Eye Res 1996; 15:533-42.
10. Taylor VL, Costello MJ. Fourier analysis of textural variations in human normal and cataractous lens nuclear fiber cell cytoplasm. Exp Eye Res 1999; 69:163-74.
11. Benedek GB. Theory of transparency of the eye. Applied Optics 1971; 10:459-73.
12. Debye P, Bueche AM. Scattering by an inhomogeneous solid. Journal of Applied Physics 1949; 20:518-25.
13. Bettelheim FA. Physical basis of lens transparency. In: Maisel E, editor. The ocular lens: structure, function, and pathology. New York: Dekker; 1985. p. 265-300.
14. Benedek GB, Pande J, Thurston GM, Clark JI. Theoretical and experimental basis for the inhibition of cataract. Prog Retin Eye Res 1999; 18:391-402.
15. van den Berg TJ. Light scattering by donor lenses as a function of depth and wavelength. Invest Ophthalmol Vis Sci 1997; 38:1321-32.
16. van den Berg TJ, Spekreijse H. Light scattering model for donor lenses as a function of depth. Vision Res 1999; 39:1437-45.
17. Boyle DL, Takemoto LJ. Confocal microscopy of human lens membranes in aged normal and nuclear cataracts. Invest Ophthalmol Vis Sci 1997; 38:2826-32.
18. Chylack LT Jr, Lee MR, Tung WH, Cheng HM. Classification of human senile cataractous changes by the American Cooperative Cataract Research Group (CCRG) method. I. Instrumentation and technique. Invest Ophthalmol Vis Sci 1983; 24:424-31.
19. Bozzola JJ, Russell LD. Electron microscopy: principles and techniques for biologists. Sudbury (MA): Jones and Bartlett; 1999.
20. Taylor VL, Al-Ghoul KJ, Lane CW, Davis VA, Kuszak JR, Costello, MJ. Morphology of the normal human lens. Invest Ophthalmol Vis Sci 1996; 37:1396-410.
21. Lo WK, Harding CV. Square arrays and their role in ridge formation in human lens fibers. J Ultrastruct Res 1984; 86:228-45.
22. Costello MJ, Oliver TN, Cobo LM. Cellular architecture in age-related human nuclear cataracts. Invest Ophthalmol Vis Sci 1992; 33:3209-27.
23. Kuszak JR, Ennesser CA, Umlas J, Macsai-Kaplan MS, Weinstein RS. The ultrastructure of fiber cells in primate lenses: a model for studying membrane senescence. J Ultrastruct Mol Struct Res 1988; 100:60-74.
24. Boyle DL, Takemoto LJ. Finger-like projections of plasma membrane in the most senescent fiber cells of human lenses. Curr Eye Res 1998; 17:1118-23.
25. Al-Ghoul KJ, Nordgren RK, Kuszak AJ, Freel CD, Costello MJ, Kuszak JR. Structural evidence of human nuclear fiber compaction as a function of ageing and cataractogenesis. Exp Eye Res 2001; 72:199-214.
26. Babizhayev MA, Deyev AI, Linberg LF. Lipid peroxidation as a possible cause of cataract. Mech Ageing Dev 1988; 44:69-89.
27. Al-Ghoul KJ, Costello MJ. Morphological changes in human nuclear cataracts of late-onset diabetics. Exp Eye Res 1993; 57:469-86.
28. Costello MJ, Marsili S, Lane CW, Salganik RI, Albright CD, Peiffer RL. Cataract formation in a strain of rats selected for high oxidative stress. Microscopy and Microanalysis 2000; 6:590-1.
29. Harding CV, Chylack LT Jr, Susan SR, Lo WK, Bobrowski WF. Elemental and ultrastructural analysis of specific human lens opacities. Invest Ophthalmol Vis Sci 1982; 23:1-13.
30. Vrensen GF, Willekens B, De Jong PT, Shun-Shin GA, Brown NP, Bron AJ. Heterogeneity in ultrastructure and elemental composition of perinuclear lens retrodots. Invest Ophthalmol Vis Sci 1994; 35:199-206.
31. VanMarle J, Vrensen GF. Cholesterol content of focal opacities and multilamellar bodies in the human lens: filipin cytochemistry and freeze fracture. Ophthalmic Res 2000; 32:285-91.
32. Harding CV, Chylack LT Jr, Susan SR, Lo WK, Bobrowski WF. Calcium-containing opacities in the human lens. Invest Ophthalmol Vis Sci 1983; 24:1194-202.
33. White TW, Goodenough DA, Paul DL. Targeted ablation of connexin50 in mice results in microphthalmia and zonular pulverulent cataracts. J Cell Biol 1998; 143:815-25.
34. Berry V, Mackay D, Khaliq S, Francis PJ, Hameed A, Anwar K, Mehdi SQ, Newbold RJ, Ionides A, Shiels A, Moore T, Bhattacharya SS. Connexin 50 mutation in a family with congenital “zonular nuclear” pulverulent cataract of Pakistani origin. Hum Genet 1999; 105:168-70.
35. Zampighi G, Simon SA, Robertson JD, McIntosh TJ, Costello MJ. On the structural organization of isolated bovine lens fiber junctions. J Cell Biol 1982; 93:175-89.
36. Costello MJ, McIntosh TJ, Robertson JD. Distribution of gap junctions and square array junctions in the mammalian lens. Invest Ophthalmol Vis Sci 1989; 30:975-89.
37. Costello MJ, Al-Ghoul KJ, Oliver TN, Lane CW, Wodnicka M, Wodnicki P. Polymorphism of fiber cell junctions in mammalian lens. In: GW Bailey and CL Rieder, editors. Proceedings of the 51st Annual Meeting of the Microscopy Society of America; 1993 August 1-6; Cincinnati, OH, USA. San Francisco: San Francisco Press; 1993. p. 200-1.

The print version of this article was created on 28 June 2001. This reflects all typographical corrections and errata to the article through that date. Details of any changes may be found in the online version of the article.